Concerted C−N/C−H Bond Formation in Highly Enantioselective Yttrium(III)-Catalyzed Hydroamination

Kuntal Manna, Marissa L. Kruse, and Aaron D. Sadow*

Department of Chemistry and U.S. DOE Ames Laboratory, Iowa State University, Ames Iowa 50011, United States

Ⓢ *Supporting Information*

ABSTRACT: A highly active oxazolinylborato yttrium hydroamination catalyst provides 2-methyl-pyrrolidines with excellent optical purities. The proposed mechanism, in which a yttrium(amidoalkene)amine complex reacts by concerted C−N and C−H bond formation, is supported by the rate law for conversion, substrate saturation under initial rates conditions, kinetic isotope effects, and isotopic perturbation of enantioselectivity. These features are conserved between oxazolinylborato Mg-, Y-, and Zr-mediated aminoalkene cyclizations, suggesting related transition states for all three systems. However, inversion of the products' absolute configuration between yttrium and zirconium catalysts coordinated by the same 4S-oxazolinylborate ligands highlight dissimilar mechanisms of stereoinduction.

KEYWORDS: hydroamination, enantioselectivity, pyrrolidine, rare-earth, organometallics, mechanism
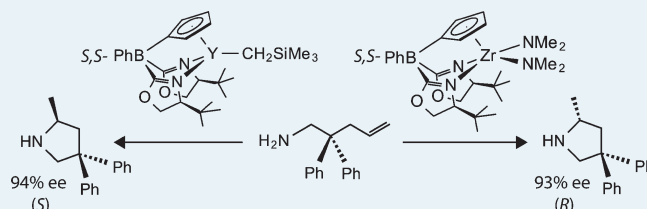
Stereochemistry is a powerful tool for mechanistic elucidation that has provided insight into a wide range of reactions, including α-olefin hydrogenation and insertion polymerization.[1−3] Early transition-metal and rare earth-catalyzed olefin hydroaminations have been shown to be related to these reactions as an insertion-based bond forming process.[4−6] Rare earth complexes stand out with very high turnover frequencies in aminoalkenes cyclizations,[7−10] as well as in insertion-based catalysis such as hydrogenation, hydrosilylation, and polymerization.[11−15] However, while models for olefin insertion into d^0 (and $f^n d^0$) M−H and M−C bonds are well developed, stereochemical studies of alkene insertions into M−N bonds are limited. Thus, stereochemical experiments could provide insight into C−N bond formations.

However, rare-earth-element-catalyzed hydroaminations are distinguished from other olefin insertions by large kinetic isotope effects (KIEs) of α-NH versus ND substitution on cyclization rates and significant isotope effects on diastereoselectivity.[8] On the basis of these observations, a proton-assisted insertion mechanism was proposed (Chart 1, A).[8,16,17] However, computational studies show low barriers for rare earth amide-mediated insertions of olefins, alkynes, and dienes without proton-assistance (Chart 1, B),[18−21] and cascade C−N/C−C bond forming reactions also suggest discrete metal−alkyl intermediates that imply direct insertion.[22]

In contrast, tris(oxazolinyl)borato-magnesium(II) and mixed cyclopentadienyl-bis(oxazolinyl)borate zirconium(IV) hydroamination catalysts were proposed to cyclize aminoalkenes through non-insertive six-center mechanisms (Chart 1, D and E).[23,24] The suggested mechanisms are based on the central role of an NH in the turnover-limiting (and in the case of the zirconium catalyst, stereochemistry-determining) C−N bond forming step. Kinetic studies also show that the proton transfer step relies on a second NH-containing ligand group for cyclization.

The six-center, proton-transfer mechanism was suggested in a Cp*(L)ZrR$_2$-catalyzed (L = salicyloxazoline) cyclization, but later ruled out in favor of a $[2\pi+2\pi]$ cycloaddition mechanism (Chart 1, C).[25] However, kinetic studies of a bis(amidate)Zr-system provide additional support for six-center transition states in aminoalkene cyclization.[26] Diketiminate group 2 catalysts follow a multisubstrate mechanism based on saturation kinetics.[27] The reactivity and catalytic activity of isolated rare earth bis(amidoalkene) compounds also suggest a concerted C−N/C−H bond forming mechanism.[28]
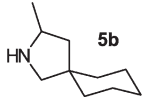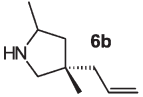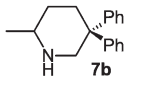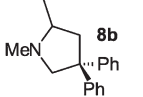
Key evidence supporting the concerted six-center mechanism in our zirconium system relied on the isotopic effect on enantioselectivity in addition to kinetic studies. Such effects have not previously been established with rare-earth-element-catalyzed hydroaminations. We now report interesting isotopic effects in yttrium-catalyzed hydroamination/cyclization as well as kinetic parameters associated with the proposed mechanism. Additionally, we have uncovered a highly active and highly enantioselective (S)-yttrium catalyst (Chart 2) for hydroamination/cyclization that provides pyrrolidine products with the mirror image of the products afforded by the (S)-zirconium catalysts. This {S-3} ligand (Chart 2) is the first system to give a range (i.e., more than two) of highly enantio-enriched pyrrolidines with rare-earth- and group 4 metal-based catalysts.

Achiral H[PhB(C$_5$H$_5$)(Ox^{Me2})$_2$][29] (**H[1]**; Ox^{Me2} = 4,4-dimethyl-2-oxazoline) and Y(CH$_2$SiMe$_3$)$_3$(THF)$_2$ react to provide {PhB(C$_5$H$_4$)(Ox^{Me2})$_2$}YCH$_2$SiMe$_3$ ({**1**}**YCH$_2$SiMe$_3$**) with the elimination of 2 equiv of SiMe$_4$. This alkyl compound decomposes by SiMe$_4$ elimination ($t_{1/2}$ = 40 min, room temperature), but analytically pure, THF-free material is obtained through recrystallization by vapor diffusion of pentane into a tetrahydrofuran

Chart 1. Transition States Proposed for C−N Bond Formation in d⁰ and fⁿd⁰-Metal Catalyzed Hydroamination
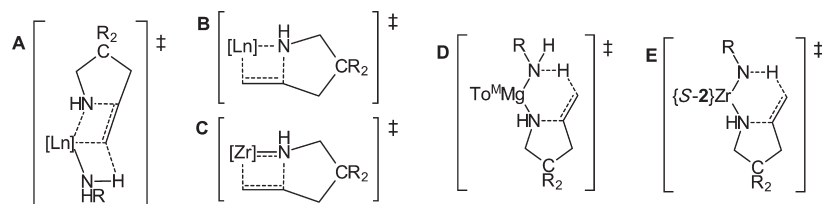
Chart 2. {PhB(C₅H₄)(OxR)₂}YCH₂SiMe₃ Precatalysts for Hydroamination/Cyclization of Aminoalkenes

{1}YCH₂SiMe₃   {S-2}YCH₂SiMe₃   {S-3}YCH₂SiMe₃
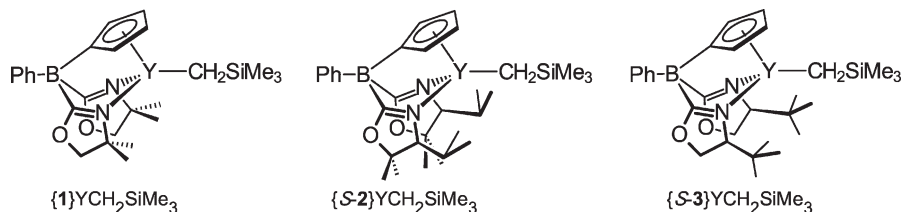
Table 1. Cyclization of Representative Aminoalkenes to Pyrrolidines and Piperidines[a]

|		{1}YR	{S-2}YR[b]	{S-2}Zr(NMe₂)₂[c]
5b	time:	10 min	10 min	1.25 h
	yield:	100%	100%	95%
	% ee:	racemic	34 (S)	90 (R)
6b	time:	25 min	10 min	30 min
	yield:	100%	100%	95%
	d.r.:	1.2:1	1.1:1	1.1:1
	% ee:	racemic	43, 40	93, 92
7b	time:	6 h	50 min	30 h
	yield:	100%	100%	65%
	% ee:	racemic	22 (S)	46 (R)
8b	time:	12 h	20 h	12 h[d]
	yield:	100%	100%	0
	% ee:	racemic	9	n.a.

[a] Conditions: 0.08 mmol of substrate, 0.5 mL of C₆D₆, r.t. [b] 5 mol % {S-2}YCH₂SiMe₃. [c] 10 mol % {S-2}Zr(NMe₂)₂, see ref 24. [d] Heated from r.t. to 170 °C in 50 °C increments for 24 h per temperature.

(THF) solution at −30 °C. One C=N band (1549 cm⁻¹, KBr) in the IR spectrum suggested that both oxazolines coordinate to the yttrium center. The compounds reported react as monomers, and related cyclopentadienyl-bis(pyrazolyl)ethane yttrium compounds are monomeric.[30] {1}YCH₂SiMe₃ is a precatalyst for primary and secondary aminoalkene cyclization at room temperature (eq 1 and Table 1).

On the basis of these results, we prepared enantiopure {PhB(C₅H₄)(S-Ox^{i-Pr,Me2})₂}YCH₂SiMe₃ ({S-2}YCH₂SiMe₃; Ox^{i-Pr,Me2} = 4S-isopropyl-5,5-dimethyl-2-oxazolinyl) using

(1)

quantitative; racemic
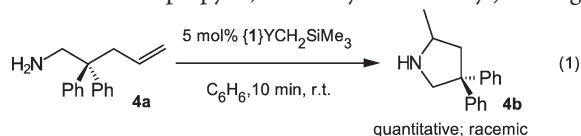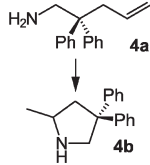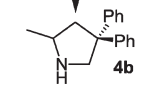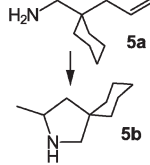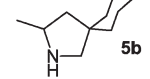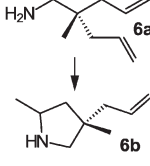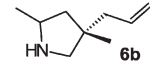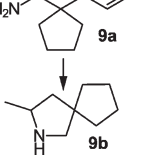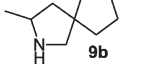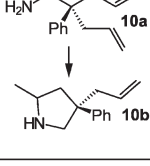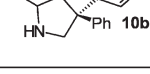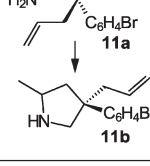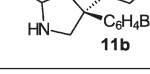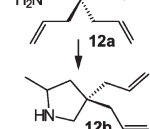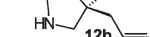
H[PhB(C₅H₅)(S-Ox^{i-Pr,Me2})₂].[24] {S-2}YCH₂SiMe₃ is C₁-symmetric as shown by four cyclopentadienyl resonances and two sets of oxazoline resonances in its ¹H NMR spectrum. The ¹⁵N NMR chemical shifts (−154.4 and −158.8 ppm) are upfield of 4S-2H-Ox^{i-Pr,Me2} (−143.3 ppm). One ν_{CN} band was observed for {S-2}-YCH₂SiMe₃ at 1558 cm⁻¹ (KBr). {S-2}YCH₂SiMe₃ is also a highly active precatalyst for aminoalkene cyclization (eq 2, Table 1).

(2)

quantitative; 42% ee; **S**
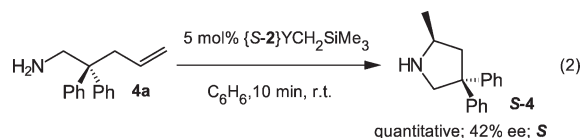
The % ee values of the pyrrolidines provided by {S-2}-YCH₂SiMe₃ are significantly lower than those obtained with

Table 2. Cyclization of Aminoalkenes and Absolute Configurations of Products for Y- and Zr-Catalyzed Hydroamination[a]

substrate/ product	catalyst[b]	time	yield[d]	% ee[c]
H_2N —… Ph Ph **4a**	$\{S\text{-}3\}YCH_2SiMe_3$	10 min	100 (93)	94 (S)
(pyrrolidine) Ph Ph N **4b**	$\{S\text{-}3\}Zr(NMe_2)_2$	18 h	95	93 (R)
H_2N —… **5a**	$\{S\text{-}3\}YCH_2SiMe_3$	10 min	100 (95)	93 (S)
(pyrrolidine) N H **5b**	$\{S\text{-}3\}Zr(NMe_2)_2$	30 h	92	87 (R)
H_2N —… **6a**	$\{S\text{-}3\}YCH_2SiMe_3$	15 min dr: 1.2:1	100 (95)	95, 95
(pyrrolidine) HN **6b**	$\{S\text{-}3\}Zr(NMe_2)_2$	30 h dr: 1.2:1	85	92, 91
H_2N —… **9a**	$\{S\text{-}3\}YCH_2SiMe_3$	3 h	95	89 (S)
(spiro pyrrolidine) N H **9b**	$\{S\text{-}3\}Zr(NMe_2)_2$	48 h	77	88 (R)
H_2N —… Ph **10a**	$\{S\text{-}3\}YCH_2SiMe_3$	15 min dr: 1.2:1	100 (96)	95, 96
(pyrrolidine) HN Ph **10b**	$\{S\text{-}3\}Zr(NMe_2)_2$	48 h dr: 2.5:1	93	88, 92
H_2N —… C_6H_4Br **11a**	$\{S\text{-}3\}YCH_2SiMe_3$	15 min dr: 1.9:1	100 (94)	95, 92
(pyrrolidine) HN C_6H_4Br **11b**	$\{S\text{-}3\}Zr(NMe_2)_2$	48 h dr: 1.2:1	90	96, 98
H_2N —… **12a**	$\{S\text{-}3\}YCH_2SiMe_3$	10 min	100 (97)	96 (S)
(pyrrolidine) HN **12b**	$\{S\text{-}3\}Zr(NMe_2)_2$	30 h	90	88 (R)

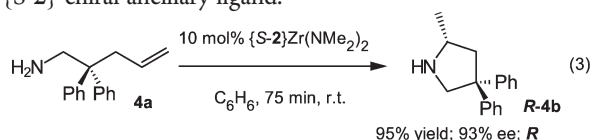[a] Reaction conditions: C_6H_6, r.t. [b] Catalyst loading Zr: 10 mol %; Y: 5 mol %. [c] The % ee values (±0.5%) were determined by ^{1}H and/or ^{19}F NMR spectroscopy of Mosher amide derivatives. Assignments of absolute configuration are based on literature reports,[16] extrapolation of ^{19}F NMR relative chemical shifts of R and S Mosher amides, and the apparent tendency of Y and Zr catalysts to provide opposite absolute configurations. [d] Yield of isolated product is given in parentheses.

$\{S\text{-}2\}Zr(NMe_2)_2$ (eq 3).[24] Surprisingly, $\{S\text{-}2\}YCH_2SiMe_3$ affords S-pyrrolidines whereas R-pyrrolidines are obtained from $\{S\text{-}2\}Zr(NMe_2)_2$ even though both catalysts contain the identical $\{S\text{-}2\}$ chiral ancillary ligand.

$$H_2N\text{–}\!\!\overset{Ph}{\underset{Ph}{\diagdown}}\ \xrightarrow[C_6H_6,\ 75\ min,\ r.t.]{10\ mol\%\ \{S\text{-}2\}Zr(NMe_2)_2}\ HN\cdots\!\!\overset{Ph}{\underset{Ph}{}}\ R\text{-}4b \quad (3)$$

4a   95% yield; 93% ee; **R**

The change in stereoinduction between $\{S\text{-}2\}Zr$- and $\{S\text{-}2\}Y$-catalyzed hydroamination/cyclizations might indicate significant mechanistic change. To verify that the configurational flip is not limited to $\{S\text{-}2\}$-based catalysts, we prepared $\{S\text{-}3\}YCH_2SiMe_3$ and $\{S\text{-}3\}Zr(NMe_2)_2$ from the new proligand $H[PhB(C_5H_5)(S\text{-}Ox^{t\text{-}Bu})_2]$ (H[S-3]; $S\text{-}Ox^{t\text{-}Bu}$ = 4S-tert-butyl-2-oxazolinyl). The ν_{CN} band at 1585 cm^{-1} (KBr) in the IR spectrum suggests that both oxazolines are

Table 3. Effect of $N\text{-}d_2$ Substitution on % ee in $\{S\text{-}3\}YCH_2SiMe_3$ and $\{S\text{-}3\}Zr(NMe_2)_2$-Catalyzed Enantioselective Hydroamination

$\{S\text{-}3\}M$ catalyst:	$[Y]CH_2SiMe_3$	$[Zr](NMe_2)_2$
4b	94 (S)	93 (R)
4b-d_2	83 (S)	96 (R)
5b	92 (S)	86 (R)
5b-d_2	87 (S)	91 (R)

coordinated in $\{S\text{-}3\}YCH_2SiMe_3$ (ν_{CN} for 4S-2H-Ox$^{t\text{-Bu}}$ is 1635 cm^{-1}).

A number of S-pyrrolidines are obtained with consistently high yields and excellent enantiomeric excesses (89−96% ee) with $\{S\text{-}3\}YCH_2SiMe_3$ as the precatalyst (Table 2). As with the $\{S\text{-}2\}M$-catalysts, $\{S\text{-}3\}YCH_2SiMe_3$ consistently provides optically active pyrrolidines with opposite absolute configurations from those obtained with $\{S\text{-}3\}Zr(NMe_2)_2$. Although these catalysts provide trisubstituted pyrrolidines with high ee's, they are less effective for preparation of piperidines and unsubstituted pyrrolidines.[31]
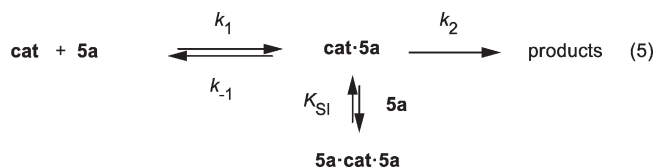
We then turned to kinetic studies to compare mechanistic features of our trivalent and tetravalent catalysts. SiMe$_4$ and pyrrolidine **5b** are observed within 30 s of addition of excess **5a** to $\{S\text{-}3\}YCH_2SiMe_3$. The rate law for the catalytic conversion of aminoalkene $-d[\mathbf{5a}]/dt = k'[\{S\text{-}3\}YCH_2SiMe_3]^1[\mathbf{5a}]^1$ ($k' = 0.105(5)$ M^{-1} s^{-1}) is established by linear first-order plots of $\ln[\mathbf{5a}]$ versus time that provide k_{obs} values and a plot of k_{obs} versus $[\{S\text{-}3\}YCH_2SiMe_3]$ that provides k' (Supporting Information, Figure S4). The rate constant k'_D for cyclization of $\mathbf{5a}\text{-}d_2$ is 0.040(5) M^{-1} s^{-1}, giving a k'_H/k'_D equal to 2.6(4). Thus, the turnover-limiting step involves N−H bond cleavage. The temperature dependence of the observed second-order rate constant k' is quantified by a plot of $\ln(k'/T)$ versus $1/T$ ($\Delta H^{\ddagger} = 7.5(3)$ kcal·mol^{-1} and $\Delta S^{\ddagger} = -38(1)$ cal·mol^{-1} K^{-1}).[32,33] These activation parameter values fall between those reported for 1-aminopent-4-ene cyclization by $(C_5Me_5)_2LaR$- and (Binol-SiPh$_3$)YR-catalyzed (Binol-SiPh$_3$ = 3,3′-bis(SiPh$_3$)-2,2′-dihydroxy-1,1′-binaphthyl) cyclizations ($\Delta H^{\ddagger} \sim 12$ to 14 kcal·mol^{-1} and $\Delta S^{\ddagger} \sim -24$ to -27 cal·mol^{-1} K^{-1})[8,16] and those obtained from 2,2-dimethyl-1-aminopent-4-ene cyclization by $Me_2Si(C_5Me_4)(Nt\text{-Bu})Th(NMe_2)_2$ ($\Delta H^{\ddagger} = 9(3)$ kcal·mol^{-1} and $\Delta S^{\ddagger} = -48(6)$ cal·mol^{-1} K^{-1}).[17]

In magnesium- and zirconium-catalyzed systems, initial cyclization rates saturate as substrate concentration increases.[23,24,27] With 5.23 mM $\{S\text{-}3\}YCH_2SiMe_3$ as precatalyst, initial cyclization rates increase over a $[\mathbf{5a}]$ range of 10.1−123 mM in a nonlinear fashion to reach saturation. The maximum rate occurs at $[\mathbf{5a}] \sim 0.06$ M. At higher $[\mathbf{5a}]$, $\{-d[\mathbf{5a}]/dt\}_{ini}$ decreases. The nonzero x-intercept that coincides with $[\{S\text{-}3\}YCH_2SiMe_3]$ indicates that 1 equiv of **5a** is required to activate the precatalyst.

A nonlinear least-squares regression analysis of the data (see Supporting Information) provides good correlation with eq 4. This rate law corresponds to the reaction mechanism shown in eq 5 that describes the initial portion of the reaction.[34]

$$-\frac{d[\mathbf{5a}]}{dt} = \frac{k_2[\{S\text{-}3\}YCH_2SiMe_3]^1\{[\mathbf{5a}] - [\{S\text{-}3\}YR]\}^1}{\{[\mathbf{5a}] - [\{S\text{-}3\}YR]\} + K' + K_{SI}\{[\mathbf{5a}] - [\{S\text{-}3\}YR]\}^2} \quad (4)$$

$$\mathbf{cat} + \mathbf{5a} \underset{k_{-1}}{\overset{k_1}{\rightleftharpoons}} \mathbf{cat\cdot 5a} \xrightarrow{k_2} \text{products} \quad (5)$$

$$K_{SI} \downharpoonleft\upharpoonright \mathbf{5a}$$

$$\mathbf{5a\cdot cat\cdot 5a}$$

The catalytic species **cat** forms from 1 equiv of **5a** and $\{S\text{-}3\}YCH_2SiMe_3$ and is modeled as equal to $[\{S\text{-}3\}YCH_2SiMe_3]$. The rate law indicates that two substrate molecules are present in $\mathbf{cat\cdot 5a}$, and its turnover-limiting conversion to products occurs with a rate constant of $k_2^H = 2.4(3) \times 10^{-2}$ s^{-1} (Supporting Information, Figure S8). Likewise, a plot of $\{-d[\mathbf{5a}\text{-}d_2]/dt\}_{ini}$ versus $[\mathbf{5a}\text{-}d_2]_{ini}$ provides a saturation curve where $k_2^D = 7.1(5) \times 10^{-3}$ s^{-1}. The value of k_2^H/k_2^D from the initial rate plots is 3.8(2), further indicating that an N−H (or N−D) bond is broken in the turnover-limiting step. Additionally, k_2^H values determined at 273, 285, 296, and 312 K provide $\Delta H^{\ddagger} = 7(3)$ kcal·mol^{-1} and $\Delta S^{\ddagger} = -40(4)$ cal·mol^{-1} K^{-1} for the turnover-limiting step. The similarity of activation parameters determined using k'_H values (for overall conversion) and k_2^H (from initial rates measurements) suggests that the turnover-limiting step probed with the initial rates method is the major contributor to the barrier for the entire catalytic cycle. This similarity also indicates that the reaction mechanism remains consistent from the initial portion through at least two half-lives.

Isotopic substitution also significantly affects the reactions' enantioselectivity. Here, the % ee's for deutero-pyrrolidines are systematically and significantly *lower* than the values for the corresponding proteo-pyrrolidines (Table 3). This enantiomeric excess decrease contrasts the $\{S\text{-}2\}Zr$- and $\{S\text{-}3\}Zr$-catalyzed hydroaminations, where the % ee *increases* upon N-deuteration of substrates. These effects show that an N−H (or N−D) bond is involved in the stereochemistry-determining step for both Zr and Y catalysts.

For $\{S\text{-}3\}YCH_2SiMe_3$, the isotope effect for the favored diastereomeric pathway (k_H^S/k_D^S) is 2.7(4) and for the unfavored diastereomers (k_H^R/k_D^R) is 1.6(3) (from k'_H/k'_D). The zirconium catalyst $\{S\text{-}2\}Zr(NMe_2)_2$ is characterized by $k'_H/k'_D =$
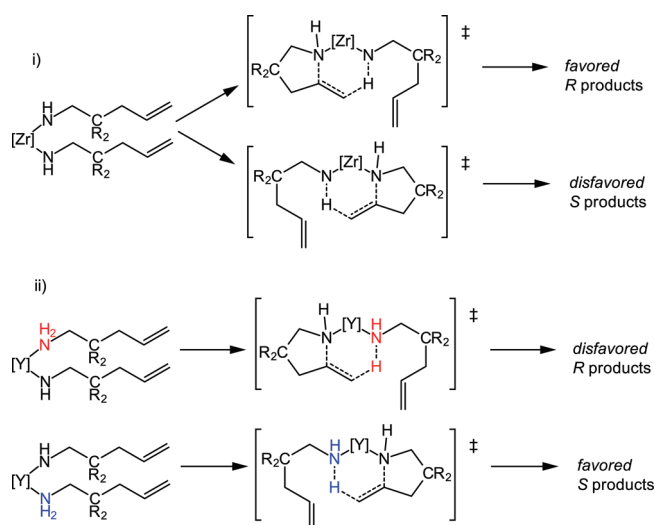
Figure 1. Proposed stereomechanism for Zr- and Y-catalyzed hydroamination.

3.5, $k_H{}^S/k_D{}^S = 7.7(1)$ and $k_H{}^R/k_D{}^R = 2.2(5)$.[24] Interestingly, *N*-deuteration slows the *S*-diastereomeric pathway by a greater extent than the *R*-pathway for both yttrium- and zirconium-catalyzed reactions. The analysis of these isotope effects provide a compelling argument that the *S* transition-states for Zr and Y catalysts are similar, as are the *R* transition-states, even though the energetically favored diastereomeric pathway are opposite.

These Y- and Zr-catalyzed hydroaminations have other similar features, including the overall rate law for substrate conversion (first-order dependence on substrate), enzyme-like rate laws from initial rate measurements, high enantioselectivity and significant primary KIEs. An achiral tris(oxazolinyl)borate magnesium catalyst also shows some of these characteristics.[23] These observations suggest that some mechanistic aspects are conserved between divalent (Mg), trivalent (Y), and tetravalent (Zr) catalysts, including the reversible catalyst-substrate association that precedes the turnover-limiting step. In all three systems, the turnover-limiting step involves N—H bond cleavage. N—H bond cleavage also significantly affects the configuration of the new stereocenter (i.e., it is associated with C—N bond formation) in the chiral Zr and Y systems. In the Mg and Y systems, the metal center's coordination number increases through an amine coordination prior to the turnover-limiting C—N bond formation, and this is unlike other insertions into M—H and M—C bonds where an open coordination site adjacent to the reacting group is required. Taken together, these observations rule out the olefin insertion mechanism for this yttrium system; the six-center transition state in which C—N and C—H bond formation occur in a concerted fashion is a reasonable alternative.

Although the general mechanistic features of the C—N bond forming step (and even the two diastereomeric transition-states) appear to be related for Zr and Y catalysts, the oppositely configured stereocenters in the catalytic products reveal that mechanisms for stereoinduction are not equivalent for Y and Zr. Our working rationalization of the stereochemistry is that the C_1-symmetric ancillary differentiates the two amidoalkenes in the transition-state in the zirconium system (Figure 1, i), whereas the configuration of the two diastereomeric intermediates {*S*-**3**}-YNHR(NH$_2$R) significantly influences the favored diastereomeric pathway in the trivalent system (ii).

This stereochemical model is obviously limited, as it does not account for chiral ancillary ligand interactions with the substrates (in the traditional fashion). However, experimental evidence that distinguishes such interactions for yttrium and zirconium are not available, and this working model highlights the change in the possible stereochemistry-determining step associated with the metal center. Therefore, our current efforts are focused on identifying the ancillary ligand—metal interactions during catalysis and synthesizing proposed intermediates to probe their stereochemistry. Despite this and other synthetic limitations, the notable increase in the range of highly enantio-enriched pyrrolidines available with mixed cyclopentadienyl bis(oxazolinyl)-borate ligands with both yttrium and zirconium highlights the potential for these ligands in enantioselective catalysis.

■ ASSOCIATED CONTENT

Ⓢ **Supporting Information.** Synthetic procedures, description of kinetics and catalytic experiments, and spectra of products. This material is available free of charge via the Internet at http://pubs.acs.org.

■ AUTHOR INFORMATION

Corresponding Author
*E-mail: sadow@iastate.edu.

■ REFERENCES

(1) Halpern, J. *Science* **1982**, *217*, 401.
(2) Clawson, L.; Soto, J.; Buchwald, S. L.; Steigerwald, M. L.; Grubbs, R. H. *J. Am. Chem. Soc.* **1985**, *107*, 3377–3378.
(3) Piers, W. E.; Bercaw, J. E. *J. Am. Chem. Soc.* **1990**, *112*, 9406–9407.
(4) Brunet, J. J.; Neibecker, D. In *Catalytic Heterofunctionalization: From Hydroamination to Hydrozirconation*; Togni, A., Grutzmacher, H., Eds.; Wiley-VCH: Weinheim, Germany, 2001; pp 91—142.
(5) Hong, S.; Marks, T. J. *Acc. Chem. Res.* **2004**, *37*, 673–686.
(6) Müller, T. E.; Hultzsch, K. C.; Yus, M.; Foubelo, F.; Tada, M. *Chem. Rev.* **2008**, *108*, 3795–3892.
(7) Gagne, M. R; Marks, T. J. *J. Am. Chem. Soc.* **1989**, *111*, 4108–4109.
(8) Gagne, M. R.; Stern, C. L.; Marks, T. J. *J. Am. Chem. Soc.* **1992**, *114*, 275–294.
(9) Giardello, M. A.; Conticello, V. P.; Brard, L.; Gagne, M. R.; Marks, T. J. *J. Am. Chem. Soc.* **1994**, *116*, 10241–10254.
(10) Tian, S.; Arredondo, V. M.; Stern, C. L.; Marks, T. J. *Organometallics* **1999**, *18*, 2568–2570.
(11) Jeske, G.; Lauke, H.; Mauermann, H.; Schumann, H.; Marks, T. J. *J. Am. Chem. Soc.* **1985**, *107*, 8111–8118.
(12) Fu, P.-F.; Brard, L.; Li, Y.; Marks, T. J. *J. Am. Chem. Soc.* **1995**, *117*, 7157–7168.
(13) Gountchev, T. I.; Tilley, T. D. *Organometallics* **1999**, *18*, 5661–5667.
(14) Watson, P. L.; Parshall, G. W. *Acc. Chem. Res.* **1985**, *18*, 51–56.
(15) Shapiro, P. J.; Cotter, W. D.; Schaefer, W. P.; Labinger, J. A.; Bercaw, J. E. *J. Am. Chem. Soc.* **1994**, *116*, 4623–4640.

(16) Gribkov, D. V.; Hultzsch, K. C.; Hampel, F. *J. Am. Chem. Soc.* **2006**, *128*, 3748–3759.

(17) Stubbert, B. D.; Marks, T. J. *J. Am. Chem. Soc.* **2007**, *129*, 6149–6167.

(18) Motta, A.; Lanza, G.; Fragala, I. L.; Marks, T. J. *Organometallics* **2004**, *23*, 4097–4104.

(19) Motta, A.; Fragala, I. L.; Marks, T. J. *Organometallics* **2006**, *25*, 5533–5539.

(20) Tobisch, S. *Chem.—Eur. J.* **2010**, *16*, 13814–13824.

(21) Tobisch, S. *Dalton Trans.* **2011**, *40*, 249–261.

(22) Li, Y.; Marks, T. J. *J. Am. Chem. Soc.* **1998**, *120*, 1757–1771.

(23) Dunne, J. F.; Fulton, D. B.; Ellern, A.; Sadow, A. D. *J. Am. Chem. Soc.* **2010**, *132*, 17680–17683.

(24) Manna, K.; Xu, S.; Sadow, A. D. *Angew. Chem., Int. Ed.* **2011**, *50*, 1865–1868.

(25) Allan, L. E. N.; Clarkson, G. J.; Fox, D. J.; Gott, A. L.; Scott, P. *J. Am. Chem. Soc.* **2010**, *132*, 15308–15320.

(26) Leitch, D. C.; Platel, R. H.; Schafer, L. L. *J. Am. Chem. Soc.* **2011**, *133*, 15453–15463.

(27) Arrowsmith, M.; Crimmin, M. R.; Barrett, A. G. M.; Hill, M. S.; Kociok-Köhn, G.; Procopiou, P. A. *Organometallics* **2011**, *30*, 1493–1506.

(28) Hangaly, N. K.; Petrov, A. R.; Rufanov, K. A.; Harms, K.; Elfferding, M.; Sundermeyer, J. *Organometallics* **2011**, *30*, 4544–4554.

(29) Manna, K.; Ellern, A.; Sadow, A. D. *Chem. Commun.* **2010**, *46*, 339–341.

(30) Otero, A.; Fernandez-Baeza, J.; Lara-Sanchez, A.; Antinolo, A.; Tejeda, J.; Martinez-Caballero, E.; Marquez-Segovia, I.; Lopez-Solera, I.; Sanchez-Barba, L. F.; Alonso-Moreno, C. *Inorg. Chem.* **2008**, *47*, 4996–5005.

(31) For reviews that summarize other rare earth element-catalyzed asymmetric hydroaminations, see refs 5 and 6. See ref 16 for highly enantioselective cyclizations of **4a** by (Binol-SiR$_3$)ScR (95% ee) and aminopent-4-ene by (Binol-SiR$_3$)LuR (92% ee).

(32) Espenson, J. H. *Chemical kinetics and reaction mechanisms*, 2nd ed.; McGraw-Hill: New York, 1995.

(33) Morse, P. M.; Spencer, M. D.; Wilson, S. R.; Girolami, G. S. *Organometallics* **1994**, *13*, 1646–1655.

(34) Cornish-Bowden, A. *Fundamentals of enzyme kinetics*, 3rd ed.; Portland Press: London, 2004.